



Enhancing the solar cell efficiency through pristine 1-dimensional SnO₂ nanostructures: Comparison of charge transport and carrier lifetime of SnO₂ particles vs. nanorods

Kosala Wijeratne^a, Jeganathan Akilavasan^a, Mukundan Thelakkat^b, Jayasundera Bandara^{a,*}

^a Institute of Fundamental Studies, Hantana Road, CP 20000, Kandy, Sri Lanka

^b Applied Functional Polymers, University of Bayreuth, 95447 Bayreuth, Germany

ARTICLE INFO

Article history:

Received 27 February 2012

Received in revised form 30 March 2012

Accepted 3 April 2012

Available online 9 April 2012

Keywords:

SnO₂ nanorods

Dye-sensitized solar cell

Charge transport

1-D structures

Charge recombination

ABSTRACT

Efficiency of dye-sensitized solar cells (DSSC) fabricated with pristine SnO₂ nanocrystals was reported to be less superior compared to DSSC based on mesoporous TiO₂ nanoparticles though both oxides have comparable electrical and surface properties. Owing to inherent high charge recombination properties of SnO₂ nanoparticles, photoanode fabricated with SnO₂ nanoparticles resulting in unexpected low open circuit voltage (V_{oc}) and fill factor (FF). To overcome inherent charge recombination in SnO₂, we investigated pristine SnO₂ nanorods and showed enhanced V_{oc} , FF and overall conversion efficiency (η) for SnO₂ nanorods. The photoanode made of SnO₂ nanorods yields nearly a 2-fold improvement in fill factor, 5 fold increases in η and a greater than 2-fold increase in short-circuit current density with a moderate increase in open-circuit photovoltage. The effects appear to arise primarily from longer electron lifetimes and reduced charge recombination of SnO₂ nanorod based solar cells compared to that of SnO₂ particles owing to 1-D nature of SnO₂ nanorod which were evaluated by open-circuit voltage decay (OCVD) and electrochemical impedance spectroscopy (EIS) methods.

© 2012 Elsevier Ltd. All rights reserved.

1. Introduction

DSSC draws a quiet attention to meet future energy demand especially in the solar energy market demanding low cost photovoltaic devices. Low cost DSSCs, introduced by B. O'Regan et al. in 1991 have reached high solar to electric power conversion efficiency currently exceeding 11% [1]. Efficiency of solar cells depends on its light harvest efficiency, the quantum yield for charge injection, and the charge collection efficiency at the electrodes [2]. Since Gratzel reported the efficient TiO₂-based DSSCs, many attempts have been made to enhance the photon–electron conversion efficiency of this low-cost solar cell [3–7]. The missionaries TiO₂ layer thickness of the working electrode of the optimized Gratzel cell is about 10 μm and consisting of a network of randomly dispersed 15–30 nm TiO₂ nanocrystals. It has been demonstrated that to improve the conversion efficiency further, it is necessary to increase the TiO₂ layer thickness [8]. However, due to the lack of a depletion layer on the TiO₂ nanocrystallite surface, a further increase in TiO₂ layer thickness results in higher electron recombination and consequently a further increase in conversion efficiency has been limited by electron recombination during the charge transport

process [9,10]. In this respect, to enhance the electron transport properties in the photoanode, a highly ordered, vertically oriented TiO₂ nanotube array of different aspect ratios and surface qualities provides better replacement to substitute the sintered TiO₂ nanoparticle films in DSSCs [11–15]. The vertical orientation of the crystalline nanotube arrays makes them excellent electron percolation pathways for efficient, vectorial charge transport along the nanotube axis. It has been reported a 6.3% efficient DSSC by growing thicker TiO₂ nanotube arrays on transparent substrates and the performance can be further improved by increasing the thickness of the TiO₂ nanotube array [16].

Alternatively, attempts have been taken to use of oxide materials with similar energy-band structure and physical properties to that of TiO₂ but with higher electronic mobility, such as ZnO [17,18] and SnO₂ [19,20] nanoparticles as an alternative to a TiO₂ photoanode in DSSCs. Despite their higher electron transport properties than that of TiO₂, the solar cell performances of the photoanode fabricated with nanoparticles of ZnO and SnO₂ were inferior to that of TiO₂ photoanode. In the case of ZnO, both nanoparticles [21–23] and 1-D structures [24] have been tested in dye sensitized solar cells. When solar cells fabricated with ZnO nanospheres and sensitized with Ru dye, the solar cells exhibit power conversion efficiency of 4.33% [21] while 1-D nanostructures of ZnO exhibits power conversion efficiency of 6% [24] which are less than TiO₂ photoanode but the results are promising. However, in the case of

* Corresponding author. Tel.: +94 81 2232002.

E-mail address: jayasundera@yahoo.com (J. Bandara).

SnO₂, only nanoparticles have been tested for DSSC and less work has been done on pristine 1-D SnO₂ structures in DSSC [25–27]. It is known that when TiO₂ is used in DSSC, the dye attached on TiO₂ surface degrades very slowly owing to the generation of e-h pair by UV light absorption [28] affecting the long term stability of DSSC. However, as the band gap of SnO₂ (3.4 eV) is larger than that of TiO₂, SnO₂ is less likely to generate holes in the VB through direct photon absorption, and devices based on SnO₂ material are more robust under UV illumination than those made from TiO₂. Therefore, the use of SnO₂ materials in anode materials in DSSC has advantage over TiO₂ [29]. However, DSSC fabricated with SnO₂ nanoparticles shows a comparatively small conversion efficiency because of the inherent fast recombination process and poor fill factor of SnO₂ particles [30]. It is well demonstrated that in SnO₂ nanoparticle based DSSC, recombination of electrons with acceptors during transit to the back contact is higher than that of TiO₂ nanoparticles [30,31]. Presence of traps seems to mediate this sort of recombination and a low effective mass (effective mass of SnO₂ and TiO₂ are ~0.1 m_e and ~10 m_e, respectively) favors both trapping and the entry of a trapped electron into a surface state [30,32]. Several attempts have been tested to enhance the conversion efficiency of SnO₂ nanoparticle based solar cells. Out of them, coating of SnO₂ nanoparticle with a very thin insulating oxide layer, such as MgO, Al₂O₃, SrTiO₃, was found to be a successful method to overcome the inherent high charge recombination in SnO₂ nanoparticles [33–35]. On the other hand, 1-D nanostructures of SnO₂ can be used to overcome high charge recombination and to achieve fast electron transport, nevertheless no attempts have been attempted to use the 1-D SnO₂ nanorod structures in DSSC. Herein we report the synthesis of 1-D SnO₂ nanostructures by simple hydrothermal method and their use in DSSC. We compared the solar cell performance of both SnO₂ nanoparticles and nanorods and the observed higher solar cell efficiency with nanorod structures are correlated with their physical and electronic properties of nanorods and nanoparticles.

2. Experimental

2.1. Materials and chemicals

FTO (Solaronix, 2 mm thick, Resistance 15 Ω/cm²), N719 dye (Dyesol), tin (IV) chloride, sodium hydroxide, ethanol, tetrapropylammonium iodide, acetonitrile, iodine and ethylene carbonate are from Sigma–Aldrich and Fisher Scientific and used as received.

2.2. SnO₂ nanorod synthesis

SnO₂ nanorods were prepared by modification of the hydrothermal method [36]. For the preparation of SnO₂ nanorods, 11.2 ml of DI water containing SnCl₄·5H₂O (0.988 g) and NaOH (0.56 g) was prepared in a beaker, and 48 ml of water–ethanol (1:1, v/v) mixture was added. Then the mixture being ultrasonically dispersed for 5 min and transferred into a 80 ml Teflon-lined autoclave that was heated to 200–210 °C and kept for 24 h. The white precipitate was collected by centrifugation after being washed with distilled water and ethanol for several times.

2.3. Preparation of electrode and fabrication of DSSC

The typical procedure of the paste making and DSSC assembling is followed to make the SnO₂ based DSSC. SnO₂ powder (300 mg), Triton X (20 μl), acetic acid (160 μl) and ethanol (2 ml) were mixed and ground well in order to obtain a paste. Doctor-bladed method was used to prepare a thin film of SnO₂ on FTO glass and it was sintered at 500 °C for 30 min. The photoelectrodes were soaked in a mixture of solution containing 0.3 mM N719 dye in ethanol for 12 h at room temperature and then washed with ethanol and dried in

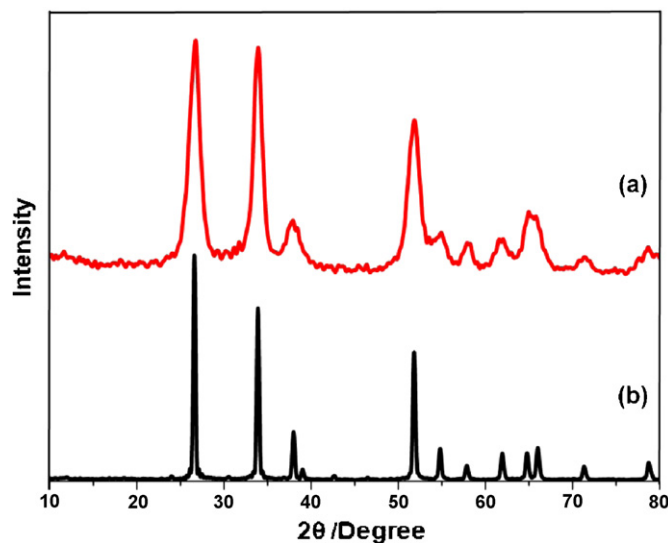


Fig. 1. XRD patterns of (a) SnO₂ nanorods and (b) SnO₂ nanoparticles.

air. Iodide/triiodide redox couple was used as an electrolyte which consisted of tetrapropylammonium iodide (0.738 g), iodine (0.06 g), ethylene carbonate (3.6 ml) and acetonitrile (1 ml).

2.4. Characterization of SnO₂ nanorods and nanoparticles

XRD measurements were carried out using powder X-ray diffraction (Bruker D8 Focus X-ray Diffractometer, with Cu K α radiation operating at 40 kV, scanning from $2\theta = 10$ to 80°). Scanning electron microscopy (SEM, LEO 1530 Gemini field emission scanning electron microscope FE-SEM and Hitachi SU6000 FE-SEM) was used to characterize the surface morphology of the thin films and powders. UV–vis absorbance spectra are measured by a Shimadzu 2450 UV–vis spectrophotometer. The current–voltage measurements of test DSSCs were performed under one sun condition using a solar light simulator (Arctron, XB 500, AM 1.5 global, 100 mW/cm²) with an active area of 0.25 cm². The intensity of the light was calibrated with a standard Si-reference cell. All efficiency values reported in this work were not corrected by the spectral mismatch factor. EIS (Zahner Zennium Electrochemical Workstation) measurements were performed under illumination (Arctron, XB 500, 100 mW/cm²) while the cell was biased at -0.4 V. The AC signal was used with amplitude of 10 mV and frequency of 0.1 Hz to 1 MHz range. For OCVD measurements, the cell was first illuminated to a steady voltage and then the open-circuit voltage decay curve was recorded once the illumination was turned off by a shutter. The above measurements were taken using Tektronix TDS 3032B Digital phosphor oscilloscope. The film thickness was measured by homemade thickness meter based on optical method and this instrument has an error of ± 2 μm.

3. Results and discussion

3.1. Characterization of SnO₂ nanorods and nanoparticles

The crystal structure of the product was firstly characterized by powder XRD method. Fig. 1 shows the powder XRD patterns from the as-prepared SnO₂ nanorod and commercially available high purity SnO₂ particles annealed in air at 500 °C. The diffraction peaks of both SnO₂ nanorods and powders are quite similar to those of bulk SnO₂, which can be indexed as the tetragonal rutile structure of SnO₂ with lattice constants of a , $b = 4.74$ Å and $c = 3.18$ Å which match well to the reported values for SnO₂ crystal

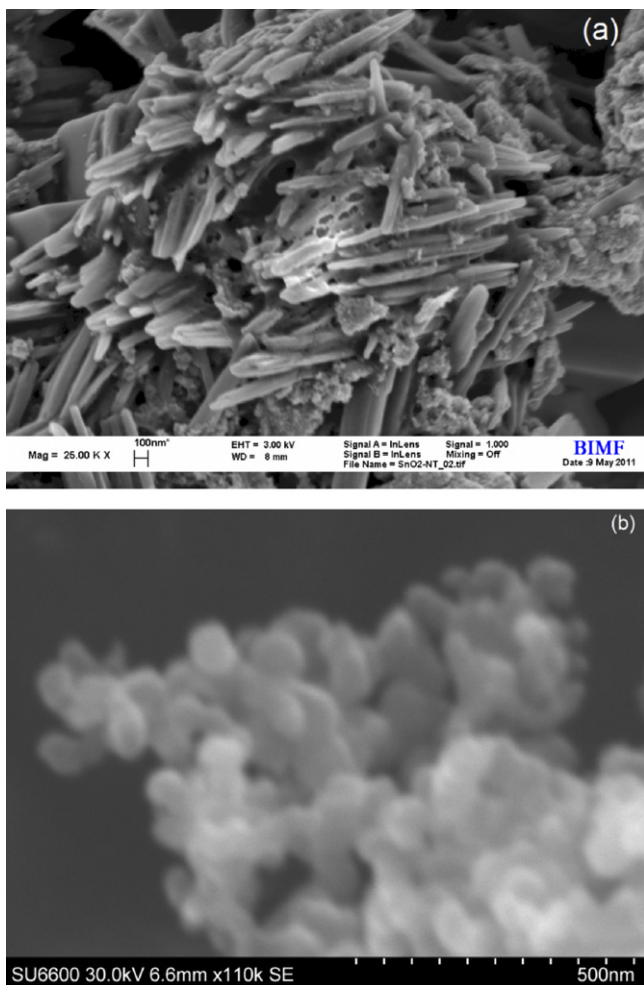


Fig. 2. SEM images of the thin film of (a) SnO₂ nanorods and (b) SnO₂ nanoparticles.

(JCPDS card, No. 41-1445). There were 8 peaks with 2θ values of 26.48, 33.87, 37.91, 38.98, 51.72, 54.85, and 57.97 and all of diffraction peaks corresponding to SnO₂ crystal planes of (110), (101), (200), (111), (211), (220), and (002), respectively. No impurity peaks were observed in both nanorods and nanoparticles, indicating the high purity of the final products. However, the diffraction peaks of SnO₂ nanorods were relatively broad compared with those of the bulk SnO₂ nanoparticles, corroborating the very small crystal size of SnO₂ nanorods. The obviously broadening of XRD peaks suggests that the as prepared SnO₂ nanorod crystals are of very small sizes. Based on the Scherrer equation, $D = 0.89\lambda / \beta \cos \theta$, here λ is the wavelength for the Cu K α (1.54056 Å), β is the full width at half maximum of the XRD peaks expressed in radian and θ is the Bragg's angle, the calculated average crystallite sizes were found to be 11.8 nm and 6.3 nm, respectively, for SnO₂ nanoparticles and nanorods based on the (211) peak. From XRD measurements, it is clear that the crystallite size of SnO₂ nanoparticles is bigger than that of SnO₂ nanorods.

Fig. 2a and b showed the typical SEM images of the thin films of SnO₂ nanorods and nanoparticles, respectively, after annealing at 500 °C for 1 h. The results showed that the diameters of the SnO₂ nanorods are around 75–100 nm with lengths of 1–2 μ m while diameter of SnO₂ nanoparticles are 50–100 nm in size. From SEM image of SnO₂ nanorods, formation of randomly oriented SnO₂ nanorods on FTO glass is clearly evident and most of the nanorods are appeared as bundles of nanorods. Fig. 3 shows the diffuse reflectance spectra of the SnO₂ nanocrystalline

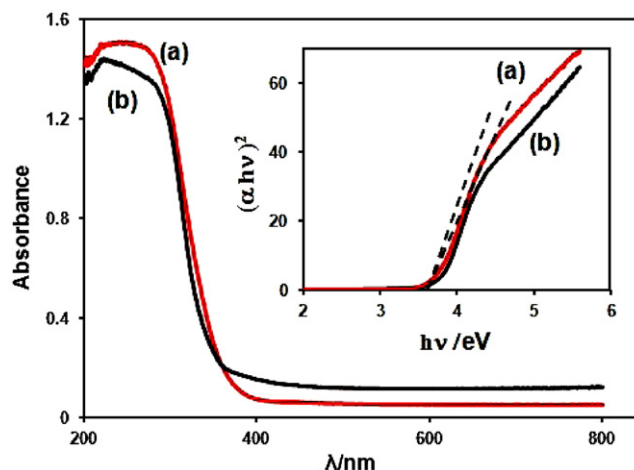


Fig. 3. Diffuse reflectance spectra of the (a) SnO₂ nanorods and (b) SnO₂ nanocrystalline powder.

powder and nanorods in the wavelength range of 800–300 nm. Both SnO₂ particles and nanorods show absorption edge around 350 nm with slightly red shifted absorption edge for SnO₂ nanorods [37]. The common feature of the both optical absorption spectra is the broadening at the absorption edge which confirms the presence of structural disorders in both nanorods and nanoparticles of SnO₂. However, higher absorption edge broadening was observed with SnO₂ nanoparticles compared to SnO₂ nanorods, which confirms the presence of greater number of structural disorders in SnO₂ nanoparticles than that of SnO₂ nanorods. The band gaps of nanorods and nanoparticles of SnO₂ were determined from the optical absorption spectra using the Tauc's procedure plotting $(\alpha hv)^2$ vs. hv and extrapolating the linear portion of absorption edge to the energy axis (inset in Fig. 3). The estimated E_g of the SnO₂ nanorods and nanoparticles is 3.70 eV and 3.77 eV, respectively. The energy positions of the SnO₂ nanorods and SnO₂ nanoparticles were measured by Mott–Schottky plot and the measured Fermi levels of the nanorods and nanoparticles are -0.2 eV and -0.32 at pH 5.5 (vs. SCE), respectively, while the estimated charge carrier densities from Mott–Schottky plots were $7.08 \times 10^{19} \text{ cm}^{-3}$ and $3.37 \times 10^{20} \text{ cm}^{-3}$ for SnO₂ nanorods and nanoparticles, respectively.

The mechanism of SnO₂ nanorod formation is probably follows the reaction paths (1) and (2) [38,39]. As a first step, Sn(OH)₄ are formed with the reaction of SnCl₄·5H₂O and NaOH solution. Sn(OH)₄ is an amphoteric hydroxide that can be dissolved in NaOH solution to form Sn(OH)₆²⁻ anion which under hydrothermal conditions hydrolysis to form SnO₂ nanorods (reaction (3)).



3.2. Solar cell performance of SnO₂ nanorods and nanoparticles

In this section, we compared the performance of solar cell fabricated with SnO₂ nanorods and nanoparticles and the observed results are correlated to the electrical properties of both SnO₂ nanorods and nanoparticles. The calculated film thickness of both films of SnO₂ nanorods and nanoparticles anode is $\sim 10 \mu\text{m}$. The current–voltage characteristics of the DSSCs based on SnO₂ nanorods and nanoparticles electrodes under the AM 1.5 G illumination at 100 mW/cm² and dark conditions are shown in Fig. 4a and b, respectively. Device fabricated with SnO₂ nanoparticles had an V_{oc} of 0.365 V, a short circuit current density (J_{sc}) of 3.2 mA/cm²

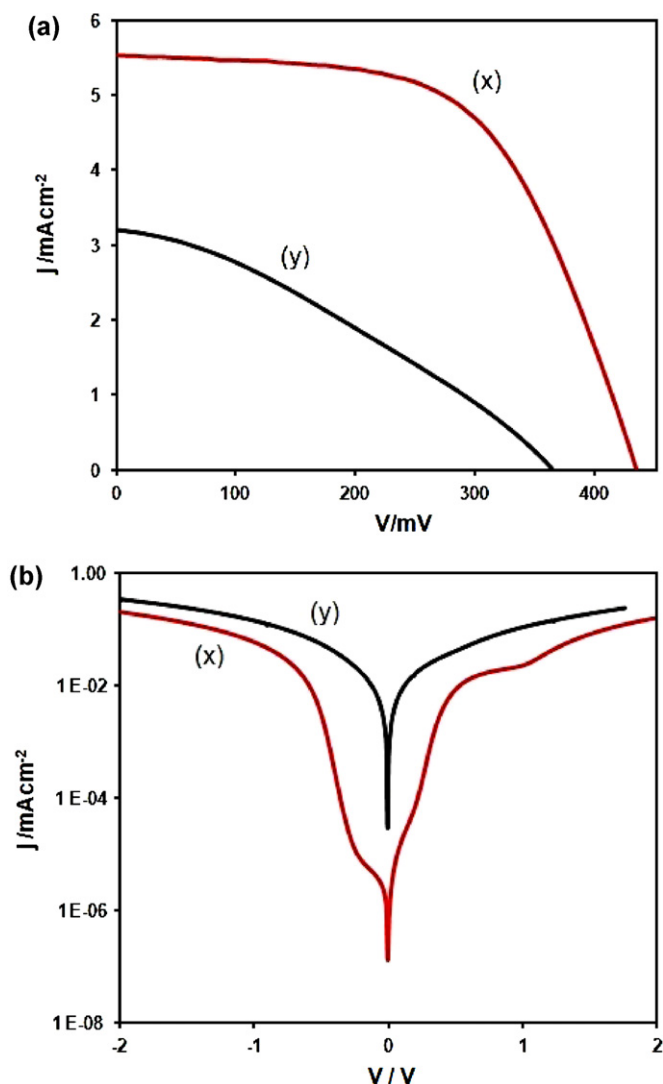


Fig. 4. (a) I - V characteristics of (x) SnO_2 nanorods and (y) nanoparticle under the AM 1.5 illumination at 100 mW/cm^2 condition. (b) I - V characteristics of (x) SnO_2 nanorods and (y) nanoparticle under dark condition.

and a FF of 32.2%, resulting in a power conversion efficiency (PCE) of 0.37% while DSSC fabricated with SnO_2 nanorods had V_{oc} , J_{sc} , FF and η of 0.435 V, 5.5 mA/cm^2 , 58.5% and 1.40%, respectively. It is clearly noticeable the increase in V_{oc} , J_{sc} and FF of the solar cell fabricated with SnO_2 nanorods compared with the solar cell performance of device fabricated with SnO_2 nanoparticles. To investigate the reason for observed higher J_{sc} for SnO_2 nanorods, we compared the dye adsorption amounts of both SnO_2 nanorods and nanoparticles and they were found to be 1.26×10^{19} and 1.92×10^{19} molecules for SnO_2 nanorods and nanoparticles, respectively. If J_{sc} is correlated to the adsorbed dye amount, higher J_{sc} is expected for the photoanode fabricated with SnO_2 nanoparticles but the J_{sc} results of SnO_2 nanoparticles and nanorods indicate different results. It can be assumed that the 1-D nature of the SnO_2 nanorods facilitates the charge transport and hence observed higher J_{sc} for photoanode fabricated with SnO_2 nanorods could be justified. The most significant difference between SnO_2 nanorods and nanoparticles is the dramatic increase in FF when SnO_2 nanorods were used as electron transport medium in the photoanode. The DSSC fabricated with SnO_2 nanoparticles in this investigation showed very poor FF and low V_{oc} and it is well documented in the literature that the photoanode fabricated with pristine SnO_2 nanoparticles exhibits very

poor FF and V_{oc} which make them not suitable as anode materials in most of the device fabrication.

It has been explained that the pristine SnO_2 has its inherent fast recombination process owing to presence of trap states which mediate the charge recombination process [30,31]. As the effective mass of SnO_2 is low compared with TiO_2 , enhanced charge recombination between photoexcited carriers in the photoanodes and tri-iodide ions in the electrolyte is common in SnO_2 particles [30,31] resulting in low FF as well as low V_{oc} and J_{sc} . Hence, use of pristine SnO_2 nanoparticles in device fabrication especially in DSSC is found to be unsuccessful. However, the DSSC fabricated with SnO_2 nanorods showed enhanced solar cell performance. As explained earlier, the most striking feature in the nanorod based device is the dramatic increase in FF to $\sim 60\%$ compared to 32% for SnO_2 nanoparticles and the reported FF and V_{oc} in this investigation are the highest FF and V_{oc} ever reported for purely SnO_2 based devices. In some cases, we have noticed that even higher FF (70%) and V_{oc} (0.55 V) could be obtained under different conditions. These results indicate that SnO_2 nanorods are better alternative for device fabrication and this could be due to its 1-D nature that enhances the electron transport while diminishing the charge recombination. In order to investigate the properties of the DSSC made of SnO_2 nanoparticles and nanorods, the series (R_s) and shunt (R_{sh}) resistances which can be obtained from the slopes of the I - V curves, were calculated from the I - V curves shown in Fig. 4 [40,41]. The calculated R_s , $(dV/dI)_{I=0}$ and R_{sh} , $(dV/dI)_{V=0}$ for SnO_2 nanoparticles based working electrode are 63.35Ω and $0.422 \text{ k}\Omega$, respectively, while calculated R_s and R_{sh} for nanorod based SnO_2 working electrodes are 24.33Ω and $1.4 \text{ k}\Omega$, respectively. It is apparent from these results that the R_{sh} of SnO_2 nanorod based films is higher than that of SnO_2 nanoparticle while R_s is smaller than that of SnO_2 nanoparticle based electrode. Higher R_{sh} resulting in lesser charge recombination and reduced R_s yielding faster charge transport are the favored conditions for an optimum device operation and hence enhanced device performance for SnO_2 nanorod based devices can be justified based on R_s and R_{sh} values. Moreover, as shown in I - V characteristic under dark conditions in Fig. 4b, the device fabricated with SnO_2 nanorod shown to exhibit lower leakage current and higher forward bias current compared to SnO_2 nanoparticles. The rectification ratios which were calculated from the current ratio at 1 V indicate that the device fabricated with SnO_2 nanorod has higher rectification ratio of 2.55 compared to SnO_2 nanoparticle based electrode which has rectification ratio of 1.32 at the same voltage. As shown above, high R_{sh} and better rectification ratio of SnO_2 nanorod, resulting in reduced leakage current and in succession DSSC fabricated with SnO_2 nanorod showed improved photovoltaic performance.

3.3. Electrochemical impedance spectroscopy analyses of the SnO_2 nanorods and nanoparticles electrodes

Electrochemical impedance measurement is a powerful tool to investigate the insight of the DSSC. We used EIS measurements to differentiate the electronic and ionic processes involved in DSSCs fabricated with SnO_2 nanorods and nanoparticles. The Nyquist plots of SnO_2 nanorod and SnO_2 nanoparticles are shown in Fig. 5 and the impedance measurements for SnO_2 nanorod and SnO_2 nanoparticles were performed by applying a 10 mV AC signal over the frequency range of 0.1 Hz to 1 MHz under one sun illumination at the bias voltage of -0.4 V . In general, impedance spectra of a DSSC show three semicircles in the frequency range $10 \mu\text{Hz}$ to 65 kHz [42]. The first, second and third semicircles from high frequency region to low frequency region correspond to the charge transfer resistance at the counter electrode, electron transport resistance and charge transfer resistance at the working electrode (electron accumulation and recombination processes in the nanocrystalline

Table 1
Electron transport properties of SnO₂ nanorods and nanoparticles determined by electrochemical impedance spectroscopy.

	R_w (Ω)	R_k (Ω)	k_{eff} (S^{-1})	τ_n (ms)	D_{eff} (cm^2/S)
SnO ₂ nanorod	0.68	119.0	35.3	28.3	6.17×10^{-5}
SnO ₂ particles	1.77	46.76	725.7	1.3	19.17×10^{-5}

film) and the electrolyte diffusion process (I^-/I_3^- in the electrolyte), respectively. In this investigation, the third semicircle is not seen and it could be obviously due to electrolyte diffusion is not significant due to the low viscous electrolyte used in this study. Hence, the semicircles seen in high frequency range in Fig. 5a could be attributed to the redox reaction at the electrolyte/Pt counter electrode interface while the mid-frequency semicircle describes the recombination process between electron in SnO₂ and the electrolyte and the short linear section at middle frequency reflects the macroscopic electron transport resistance in SnO₂. The electronic parameters of the SnO₂ electrodes were derived by fitting the impedance data of Nyquist plots shown in Fig. 5 by using the equivalent circuit according to the diffusion-recombination model shown in inset in Fig. 5 and the results are shown in solid line in Fig. 5 [43,44]. Electron transport parameters, such as electron transport resistance (R_w), charge recombination resistance (R_k), effective rate constant for recombination ($k_{\text{eff}} = \omega_k$), effective electron diffusion coefficient (D_{eff}) and life time (τ_n), were derived from the Nyquist plots of SnO₂ nanorods and nanoparticles according to the procedure demonstrated by Adachi et al. are given in Table 1.

The estimated electrons transport resistances of SnO₂ nanoparticle and nanorods are 1.77 and 0.68 Ω , respectively, indicating that SnO₂ nanorod exhibits lower electron transport resistance and the same property leading to higher solar cell efficiency in SnO₂ nanorod based DSSC. The observed lower R_w of SnO₂ nanorod can be attributed to the 1-D nature of the SnO₂ nanorod, as it provides a direct conduction path for electrons injected from the sensitizing dye. Hence, it is expected to reduce the electron diffusion time from the point of injection to the back contact in SnO₂ nanorods. However, electron transport in SnO₂ nanoparticles proceeds in a random pathway by a trap-limited diffusion process. Due to trap limited diffusion process in SnO₂ nanoparticles, the electrons must pass through a series of inter-particle hopping steps (estimated in 10^3 – 10^6 particles), in order to reach the collection electrode. Hence,

observed higher R_w for SnO₂ nanoparticle justified why DSSC fabricated with SnO₂ particles shows inferior solar cell performance. Furthermore, lower FF reported for the DSSC fabricated with SnO₂ nanoparticles electrode also could be attributed to the high R_w associated with the SnO₂ nanoparticles. The most striking feature observed from EIS measurement was the charge recombination resistance difference between SnO₂ nanoparticle and nanorods as shown in mid-frequency semicircle. The mid-frequency semicircle in Fig. 5 for SnO₂ nanorods is larger than that of SnO₂ nanoparticles and the enlarged mid-frequency arc represents a reduced recombination process in SnO₂ nanorods. As given in Table 1, R_k of SnO₂ nanorods and nanoparticles is 119.0 Ω and 46.76 Ω , respectively, which clearly indicates higher charge recombination with the electrode fabricated with SnO₂ nanoparticles compared to SnO₂ nanorods. The smaller R_k in the SnO₂ nanoparticle which indicates the more abundant electron interfacial recombination occurring is consistent with the observation of the lower FF in the cell in comparison with the SnO₂ nanorods. It has been demonstrated that even though, electron transport property of SnO₂ nanoparticles is superior to that of TiO₂ nanoparticles, DSSC fabricated with pristine SnO₂ nanoparticles exhibits very poor solar cell performance mainly owing to its known higher charge recombination process arising from its lower effective electron mass [30,31]. However, DSSC fabricated with SnO₂ nanorods exhibits higher solar cell performance as the charge recombination is greatly reduced when SnO₂ nanorods are used as electron transport medium in DSSC.

Furthermore, τ_n which was extracted from the frequency at the middle frequency peak in the Bode-phase plots using $\tau = 1/2\pi f_{\text{max}}$ also clearly indicates the higher electron life-time for injected electrons in SnO₂ nanorod than that of SnO₂ nanoparticles. Maximum frequency of SnO₂ nanorod (f_{max} , 5.62 Hz, $\tau_n = 0.028$ s) shifts to a lower frequency compared with SnO₂ nanoparticle ($f_{\text{max}} = 115.5$ Hz, $\tau_n = 0.0013$ s), corresponding to an increase in the electron lifetime for SnO₂ nanorod based DSSC and increased τ could be attributed to the 1-D nature of SnO₂ leading to higher solar cell performance with the SnO₂ nanorods. Hence with EIS investigation, we showed the enhanced electron transport properties, reduced charge recombination and increased electron life-time which are imperative for higher solar cell performance could be achieved using pristine SnO₂ nanorod.

3.4. Open circuit voltage decay (OCVD) measurement study of SnO₂ nanorods and nanoparticles electrode

To investigate the electronic process of the recombination in SnO₂ nanorods and nanoparticles further, we used OCVD measurements [45]. Employing OCVD method, minority carrier lifetime could be determined by measuring the decay of the V_{oc} after ceasing off the illumination and the voltage decay can be transformed into electron lifetime, τ_n according to the following equation:

$$\tau_n = -\frac{k_B T}{q} \left(\frac{dV_{\text{oc}}}{dt} \right)^{-1}$$

where k_B is the Boltzmann constant, T is the temperature, and q is the elementary charge. In OCVD measurements, the transport resistance in the film does not affect the measurements given that there is no current flowing through the cell due to its open-circuit condition.

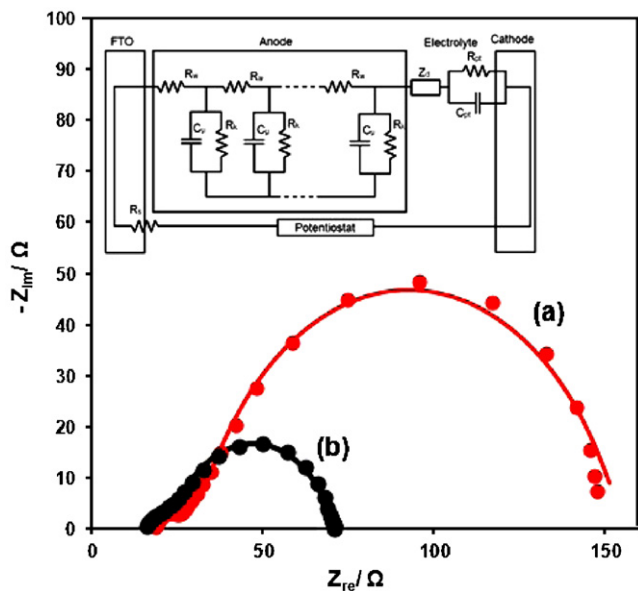


Fig. 5. Nyquist plot of impedance data for (a) SnO₂ nanorods and (b) SnO₂ nanoparticle under illumination at 1 sun and -0.4 V bias conditions.

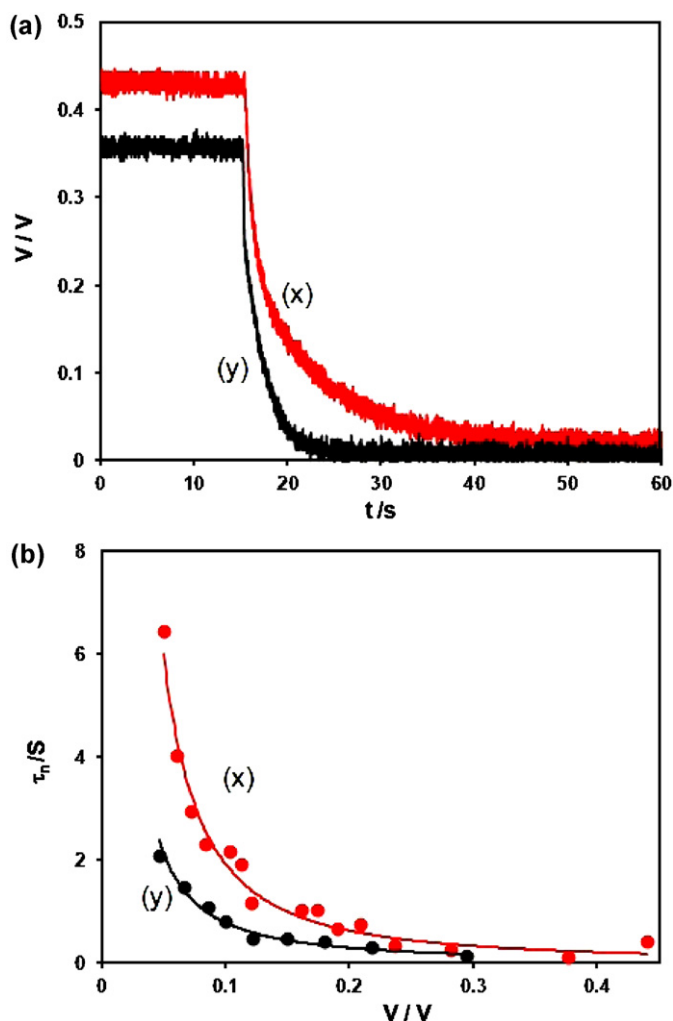


Fig. 6. (a) Voltage decay measurements of SnO₂ (x) nanorods and (y) nanoparticles and (b) the calculated electron life time as function of voltage.

Voltage decay measurements of SnO₂ nanorods and nanoparticles are shown in Fig. 6a and the calculated electron lifetime as a function of voltage is shown in Fig. 6b. As shown in Fig. 6b, for both SnO₂ nanorods and nanoparticles, the observation that the almost exponential increases in τ_n with decreasing voltage is in excellent agreement to the previous results. The measured τ_n by OCVD method consists of an average time for survival of free and trapped electrons than the free carrier lifetime. The electron lifetime under open-circuit conditions is longer in the DSSC fabricated with SnO₂ nanorod compared to SnO₂ nanoparticles indicating that 1-D nature is effective in decreasing the charge recombination rate at the interface.

Interestingly, the life times in the SnO₂ nanorods are much higher than those in the SnO₂ nanoparticles in the low V_{oc} region while the difference in lifetime is not dramatic in high V_{oc} region. It is known that the lifetime of the electron in the low voltage region depends on the surface trap density in the photoanode and higher lifetime in low V_{oc} region with SnO₂ nanorod indicates that SnO₂ nanorod possesses a lower surface trap density and hence reduced charge recombination rates compared with SnO₂ nanoparticles. Similarly, the lower surface trap density of SnO₂ nanorod is consistent with the higher FF observed in the SnO₂ nanorod DSSC. Hence, the observation extracted from OCVD measurements indicates that lower surface trap density and enhanced electron lifetime for the device fabricated with SnO₂ nanorod substantiate the higher

solar cell performance with SnO₂ nanorod than SnO₂ nanoparticles. Furthermore, earlier by Mott–Schottky plots we noted the higher charge carrier density for SnO₂ nanoparticle than SnO₂ nanorod. As higher charge carrier density enhances the charge recombination, observed lower FF and higher charge recombination for SnO₂ nanoparticles was further justified.

The results presented in this investigation clearly suggested that 1-D nature of SnO₂ is beneficial for efficient electrons transport and suppression of charge recombination in solar cell fabricated with SnO₂ nanorods compared to SnO₂ nanoparticles. However, the literature revealed that both liquid and solid type DSSCs fabricated with 1-D TiO₂ structures, such as TiO₂ nanotube and nanorods, could not exceed the highest efficiency reported for solar cells fabricated with mesoporous TiO₂ nanoparticles [16,45,46]. As explained earlier, the effective electron mass of SnO₂ nanoparticles is lower than that of TiO₂ nanoparticles, the conduction band electrons in SnO₂ get trapped and transferred easily to an acceptor state at the surface resulting in high charge recombination as well as low efficiency [30,31]. Therefore, DSSCs fabricated with 1-D structures such as SnO₂ nanorods which provide direct and enhanced charge transport while minimizing charge recombination results in enhanced efficiency in SnO₂ nanorod based DSSCs compared to SnO₂ nanoparticles. Transport and recombination studies of TiO₂ nanoparticles, oriented and randomly packed TiO₂ nanotubes showed similar electron transport times for all nanoparticles and rods whereas charge recombination was suppressed in nanotubes/rods indicating enhanced charge collection efficiency of the TiO₂ nanotube electrode [47,48]. Despite, TiO₂ nanoparticles comparatively having higher charge recombination rates than that of TiO₂ nanotubes, charge recombination is better suppressed in TiO₂ nanoparticles based DSSCs than that of SnO₂ nanoparticles based DSSCs as the effective electron mass of TiO₂ nanoparticles is high (the electrons in the conduction band are less likely to get trapped in TiO₂) [30,31]. Hence, probably due to lower charge recombination in TiO₂ nanoparticles than that of SnO₂ nanoparticles, the efficiency of DSSC fabricated with TiO₂ nanoparticles is high enough for practical application.

4. Conclusion

It was demonstrated for the first time that the pristine SnO₂ nanorods with fast electron transport properties and reduced charge recombination rates can be employed as anode materials in DSSC successfully. The overall power conversion efficiency of the SnO₂ nanorods DSSC reaches to ~1.5% with the highest reported FF for unaltered SnO₂ materials. Enhanced solar cell performance of device fabricated with the SnO₂ nanorods could be attributed to 1-D nature of the SnO₂ nanorods that enhances electron transport as well as electron lifetime. The longer electron lifetimes observed for SnO₂ nanorods means lower charge recombination which is beneficial for solar cell performance. Furthermore, the electrode fabricated with pristine SnO₂ nanoparticles is not suitable as anode material in DSSC due to presence of higher number of surface states hence charge carrier density leading to enhanced charge recombination.

Acknowledgments

A research grant from AvH Foundation, Germany to purchase electrochemical workstation is highly appreciated. Support from Visiting Professor Program and Sustainable Energy Technology, Department of Electrical Engineering of King Saud University, Riyadh, KSA are highly appreciated. MT acknowledges financial support from SFB 840.

References

- [1] M.K. Nazeeruddin, P. Péchy, T. Renouard, S.M. Zakeeruddin, R. Humphry-Baker, P. Comte, P. Liska, L. Cevey, E. Costa, V. Shklover, L. Spiccia, G.B. Deacon, C.A. Bignozzi, M. Grätzel, *Journal of the American Chemical Society* 123 (2001) 1613.
- [2] M. Grätzel, *Journal of Photochemistry and Photobiology A: Chemistry* 164 (2004) 3.
- [3] Y. Li, J. Hagen, W. Schaffrath, P. Otschik, D. Haarer, *Solar Energy Materials and Solar Cells* 56 (1998) 167.
- [4] K. Hara, T. Horiguchi, T. Kinoshita, K. Sayama, H. Sugihara, H. Arakawa, *Chemistry Letters* 4 (2000) 16.
- [5] C. Nasr, P.V. Kamat, S. Hotchandani, *Journal of Physical Chemistry B* 102 (1998) 10047.
- [6] X. Dou, D. Sabba, N. Mathews, L.H. Wong, Y.M. Lam, S. Mhaisalkar, *Chemistry of Materials* 23 (2011) 3938.
- [7] N. Takahiro, H. Hajime, A. Masahiro, W. Xing-Zheng, O. Takashi, *Key Engineering Materials* 388 (2009) 293.
- [8] S. Ito, M.K. Nazeeruddin, S.M. Zakeeruddin, P. Péchy, P. Comte, M. Grätzel, T. Mizuno, T. Koyanagi, *International Journal of Photoenergy* (2009) 517609.
- [9] G. Hodes, I.D.J. Howell, L.M. Peter, *Journal of the Electrochemical Society* 139 (1992) 3136.
- [10] M. Grätzel, *Nature* 414 (2001) 338.
- [11] P. Roy, D. Kim, K. Lee, E. Spiecker, P. Schmuki, *Nanoscale* 2 (2010) 45.
- [12] J. Bandara, K. Shankar, J. Basham, H. Wietasch, M. Paulose, O.K. Varghese, C.A. Grimes, M. Thelakkat, *European Journal of Applied Physics* 53 (2011) 20601.
- [13] N.K. Allam, X.J. Feng, C.A. Grimes, *Chemistry of Materials* 20 (2008) 6477.
- [14] H. Wang, C.T. Yip, K.Y. Cheung, A.B. Djurišić, M.H. Xie, Y.H. Leung, W.K. Chan, *Applied Physics Letters* 89 (2006) 023508.
- [15] K. Yu, J. Chen, *Nanoscale Research Letters* 4 (2009) 1.
- [16] K. Shankar, J. Bandara, M. Paulose, H. Wietasch, O.K. Varghese, G.K. Mor, T.J. LaTempa, M. Thelakkat, C.A. Grimes, *Nano Letters* 8 (2008) 1654.
- [17] E.M. Kaidashev, M. Lorenz, H. von Wenckstern, A. Rahm, H.C. Semmelhack, K.H. Han, G. Benndorf, C. Bundesmann, H. Hochmuth, M. Grundmann, *Applied Physics Letters* 82 (2003) 3901.
- [18] J. Hart, Y.-B. Cheng, G.P. Simon, L. Speccia, *Journal of Nanoscience and Nanotechnology* 8 (2008) 2230.
- [19] Z.M. Jarzebski, J.P. Marton, *Journal of Electrochemical Society* 123 (1976) 299C.
- [20] N. Tsuda, K. Nasu, A. Yanase, K. Siratori, *Electronic Conduction in Oxides*, Springer, Berlin/Heidelberg, 1991.
- [21] K. Keis, J. Lindgren, S.E. Lindquist, A. Hagfeldt, *Langmuir* 16 (2000) 4688.
- [22] K. Kakiuchi, E. Hosno, S. Fujihara, *Journal of Photochemistry and Photobiology A: Chemistry* 79 (2006) 81.
- [23] H.M. Cheng, W.H. Chiu, C.H. Lee, S.Y. Tsai, W.F. Hsieh, *Journal of Physical Chemistry C* 112 (2008) 16359.
- [24] M. Law, L.E. Green, J.C. Johnson, R. Saykally, P. Yang, *Nature Materials* 4 (2005) 455.
- [25] Y. Fukai, Y. Kondo, S. Mori, E. Suzuki, *Electrochemistry Communications* 9 (2007) 1439.
- [26] S. Gubbala, H.B. Russell, H. Shah, B. Deb, J. Jasinski, H. Rypkema, M.K. Sunkara, *Energy Environmental Science* 2 (2009) 1302.
- [27] S. Gubbala, V. Chakrapani, V. Kumar, M.K. Sunkara, *Advanced Functional Materials* 18 (2008) 2411.
- [28] H.G. Agrell, J. Lindgren, A. Hagfeldt, *Solar Energy* 75 (2003) 169.
- [29] P. Tiwana, P. Docampo, M.B. Johnston, H.J. Snaith, L.M. Herz, *ACS Nano* 5 (2011) 5158.
- [30] K. Tennakone, P.K.M. Bandaranayake, P.V.V. Jayaweera, A. Konno, G.R.R.A. Kumara, *Physica E* 14 (2002) 190.
- [31] P.V.V. Jayaweera, A.G.U. Perera, K. Tennakone, *Inorganica Chimica Acta* 361 (2008) 707.
- [32] D.W. Kormann, M.R. Bahnemann, M. Hoffmann, *Journal of Physical Chemistry* 92 (1988) 5196.
- [33] K. Tennakone, J. Bandara, P.K.M. Bandaranayake, G.R.A. Kumara, A. Konno, *Japanese Journal of Applied Physics Part 2: Letters* 40 (2001) L732.
- [34] C. Prasittichai, J.T. Hupp, *Journal of Physical and Chemical Letters* 1 (2010) 1611.
- [35] W. Chen, Y. Qiu, Y. Zhong, K.S. Wong, S. Yang, *Journal of Physical Chemistry A* 114 (2010) 3127.
- [36] X. Xue, L. Xing, Y. Chen, S. Shi, Y. Wang, T. Wang, *Journal of Physical Chemistry C* 112 (2008) 12157.
- [37] E.A. Floriano, L.V.A. Scalvi, J.R. Sambrano, V. Geraldo, *Materials Research* 13 (2010) 437.
- [38] Q.T. Khuc, X.H. Vu, D.V. Dang, D.C. Nguyen, *Advance Nature Science: Nanoscience and Nanotechnology* 1 (2010) 25010.
- [39] K. Ishibashi, Y. Kimura, M. Niwano, *Journal of Applied Physics* 103 (2008) 094507.
- [40] A.F. Nogueira, M.A. De Paoli, I. Montanari, R. Monkhose, J. Nelson, J.R. Durrant, *Journal of Physical Chemistry B* 105 (2001) 7517.
- [41] R. Kern, R. Sastrawan, J. Ferber, R. Stangl, J. Luther, *Electrochimica Acta* 47 (2002) 4213.
- [42] F. Fabregat-Santiago, G. Garcia-Belmonte, I. Mora-Sero, J. Bisquert, *Physical Chemistry Chemical Physics* 13 (2011) 9083.
- [43] M. Adachi, M. Sakamoto, J. Jiu, Y. Ogata, S. Isoda, *Journal of Physical Chemistry B* 110 (2006) 13872.
- [44] A. Zaban, M. Greenshtein, J. Bisquert, *Chemical Physics Chemistry* 4 (2003) 859.
- [45] J. Bandara, K. Shankar, J. Basham, H. Wietasch, M. Paulose, O.K. Varghese, C.A. Grimes, M. Thelakkat, *European Physical Journal Applied Physics* 53 (2011) 20601.
- [46] J. Wang, Z. Lin, *Chemistry of Materials* 22 (2010) 579.
- [47] Y. Ohsaki, N. Masaki, T. Kitamura, Y. Wada, T. Okamoto, T. Sekino, K. Niihara, S. Yanagida, *Physical Chemistry Chemical Physics* 7 (2005) 4157.
- [48] K. Zhu, N.R. Neale, A. Miedaner, A.J. Frank, *Nano Letters* 7 (2005) 69.